Bioelectrochemistry 155 (2024) 108571

Contents lists available at ScienceDirect

Bioelectrochemistry

journal homepage: www.journals.elsevier.com/bioelectrochemistry

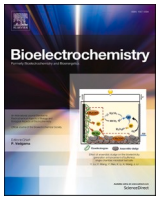

Angiogenesis inhibitor or aggressiveness marker? The function of endostatin in cancer through electrochemical biosensing

Sandra Tejerina-Miranda [a], María Pedrero [a], Marina Blázquez-García [a], Verónica Serafín [a], Ana Montero-Calle [b], Maria Garranzo-Asensio [b], A. Julio Reviejo [a], José M. Pingarrón [a], Rodrigo Barderas [b], Susana Campuzano [a,*]

[a] Departamento de Química Analítica, Facultad de CC. Químicas, Universidad Complutense de Madrid, Pza. de las Ciencias 2, 28040 Madrid, Spain
[b] Chronic Disease Programme, UFIEC, Institute of Health Carlos III, Majadahonda, 28220 Madrid, Spain

ARTICLE INFO

Keywords:
Electrochemical bioplatform
Endostatin
Angiogenesis
Colorectal cancer aggressiveness
Tissue
Plasma

ABSTRACT

This work reports the first electrochemical bioplatform developed for the determination of human endostatin (HE), a biomarker with recognized antiangiogenic potential whose elevated circulating levels have also been associated with the development of aggressive cancers. The developed electroanalytical biotool combines the benefits of using magnetic microparticles for the implementation of sandwich immunoassays and amperometric transduction on disposable carbon electrodes. A limit of detection (LOD) of 34.1 pg mL^{-1} for HE standards and a selectivity suitable for its foray into the clinical oncology area, are demonstrated. The determination of HE in clinical samples such as lysates and secretomes of colorectal cancer (CRC) cells, plasma, and tissue samples from patients with CRC in different stages, has been faced with satisfactory results showing the ability for discriminating the metastatic capabilities of cells and for identifying and staging CRC patients. The developed bioplatform allows precise quantitative determinations, requiring minimal pre-treatments and sample amounts in only 75 min. In addition, due to the instrumentation and the type of substrates used in the detection step, the biotool is compatible with implementation in multiplexed and/or point-of-need devices, features in which this bioplatform is advantageous with respect to the enzyme linked immunosorbent assay (ELISA) or immunoblotting technologies.

1. Introduction

Angiogenesis, defined as the growth of new blood vessels from pre-existing vasculature providing tissues with oxygen and nutrients, is fundamental to many pathophysiologic processes, including neoplastic diseases and non-neoplastic diseases such as embryogenesis and tissue regeneration. Moreover, the growth of solid tumours depends on angiogenesis to allow increased oxygen requirements and nutrient supply for tumour cells to survive and proliferate [1].

Endostatin, discovered in 1997 by O'Reilly et al. [2], is a 20 kDa globular C-terminal fragment of type XVIII collagen, an extracellular matrix protein. It is highly studied as a potent inhibitor of angiogenesis as well as for its anti-atherosclerotic effect [1]. It has been described that endostatin can inhibit angiogenesis by heparin-dependent or -independent mechanisms at high and picomolar endostatin concentrations, respectively [3]. During endothelial activation, recombinant endostatin is released, blocking angiogenesis, suppressing primary tumour growth, inhibiting cell migration, and inducing apoptosis and cell-cycle arrest, thus leading to reduced vascularization of tumours. A genetic loss of normal physiological endostatin levels enhances angiogenesis and increases tumour growth [4]. Endostatin levels can be systematically increased in renal disease, cardiovascular disease and some malignancies, where circulating endostatin is a biomarker of disease onset/progression. However, it is down-regulated especially in tissue repair, wound healing, and chronic inflammation, where local endostatin depletion may be beneficial for organ/tissue recovery. Moreover, endostatin may prevent the progression of atherosclerosis (AS) and myocardial infarction (MI) [5]. Endostatin is not only a biomarker of angiogenesis, but also a hormone that regulates these processes, and has been widely used in the antiangiogenic therapy of melanoma tumour, hepatoma, breast cancer, and colorectal cancer (CRC). It has been reported that treatment of lung, gastric, oesophageal, colorectal, and

* Corresponding author.
E-mail address: susanacr@quim.ucm.es (S. Campuzano).

https://doi.org/10.1016/j.bioelechem.2023.108571
Received 8 August 2023; Received in revised form 2 September 2023; Accepted 13 September 2023
Available online 14 September 2023

breast cancer with endostatin associated with conventional therapy induced a significant improvement in patient prognosis compared to treatment with chemoradiotherapy. However, endostatin pharmacologic strategies for renal or cardiovascular diseases (CVDs) are still at a very early stage [3,5]. Physiologic levels of serum endostatin are within the range ~40–100 ng mL^{-1}. Some studies have found high levels of endostatin to be associated with the development of aggressive cancers and, therefore, with worse prognosis [1]. Thus, for example, CRC patients with liver metastases showed plasma endostatin levels of (71.6 ± 28.6) ng mL^{-1}, while concentrations of (43.2 ± 15.1) ng mL^{-1} were found for controls [6]. A cut-off value of 172 ng mL^{-1} in serum of CRC patients has been established [7]. On the other hand, concentration levels of (0.2–20 mg mL^{-1}) have been claimed to be effective in the inhibition of tumour growth [8].

The significant role of endostatin in angiogenesis and tumour growth has led to the development of ELISA methods for its evaluation as a biomarker in various cancers and other diseases [9]. Mass spectrometry (MS) [10,11], surface plasmon resonance (SPR) [12], Western blot, and immunohistochemistry [13] have also been used for its isolation and identification or detection. In most cases, these technologies are high reagent consuming, complex, use expensive equipment and need qualified staff. On the other hand, up to date no electrochemical sensors for endostatin determination have been reported. In fact, currently, the standardized method for the detection of endostatin is ELISA and several kits are commercially available. They have been applied to the diagnosis of malignant pleural effusion, the prediction of overall survival of hepatocellular carcinoma patients [14] and, more recently, to the analysis of this biomarker, in comparison with others, as prediagnostic biomarker in blood plasma for early detection of pancreatic cancer [15].

Although some ELISA kits for the determination of endostatin claim dynamic ranges from as low as 10 pg mL^{-1} and up to 10 ng mL^{-1} (Sigma Aldrich-RAB0095 and Invitrogen-EHCOL18A1), the determination involves expensive non-portable instrumentation. Considering the great interest attracted by electrochemical immunoplatforms in the development of simple low-cost systems for the sensitive and specific determination of clinical biomarkers with potential for their implementation in personalized medicine tests [16], we report in this work the first immunoplatform so far for the determination of human endostatin (HE). The method involves a sandwich immunomagnetic configuration implemented on a disposable amperometric system and shows an attractive performance in terms of sensitivity and selectivity as well as the ability to be applied in complex clinical samples of different nature, such as cancer cells, plasma, secretomes, and tissues from healthy individuals and CRC patients.

2. Experimental section

2.1. Apparatus and electrodes

A CHI1140A potentiostat (CH Instruments) operated by CHI1140A software, screen-printed carbon electrodes (SPCEs, DRP-110) and their connecting cable (DRP-CAC) purchased from Metrohm Hispania were used for electrochemical measurements. A magnetic particle concentrator (DynaMag-2, Cat. No: 12321D, Dynabeads®, Invitrogen™ Thermo Fisher Scientific) was used to separate and manipulate magnetic microbeads (MBs) that were captured after modification on the SPCE working electrode after placing it in a homemade polymethylmethacrylate (PMMA) housing with a Nd magnet (⌀ 4 × 4 mm, AIMAN GZ) embedded.

A uniform temperature incubator shaker (Thermo-shaker MT100, Universal Labortechnik), a Bunsen AGT-9 Vortex, an MPW-65R centrifuge from MPW (Med. Instruments), a Crison model Basic 20 + pH-meter and a Velp Scientifica srl magnetic stirrer were also employed.

2.2. Reagents and solutions

All used reagents were of the highest available grade. Carboxylic acid-modified-magnetic beads (HOOC-MBs, Dynabeads™, Cat. No.: M-270, 2.8 μm ⌀, ~2×10^9 beads mL^{-1}) were acquired from Invitrogen™ Thermo Fisher Scientific. N-(3-dimethyl-aminopropyl)-Ń-ethyl-carbodiimide (EDC), N-hydroxysulfosuccinimide (Sulfo-NHS), ethanolamine (ETA), hydroquinone (HQ) and hydrogen peroxide (H_2O_2, 30 % v/v) were purchased from Sigma-Aldrich. Commercial Blocker™ Casein in PBS (BB) was from Thermo Scientific (Cat. No. 37528). Sodium chloride, potassium chloride, sodium di-hydrogen phosphate, di-sodium hydrogen phosphate, 2-(N-morpholino)ethanesulfonic acid (MES) and Tris-hydroxymethyl-aminomethane-HCl (Tris-HCl) were acquired from Scharlab.

Water purified by a Milli-Q purification system (18.2 MΩ cm) was used for the preparation of all employed buffer solutions: 0.025 mol L^{-1} MES buffer pH 5.0; 0.1 mol L^{-1} Tris-HCl pH 7.2; 0.01 mol L^{-1} phosphate buffer saline solution (PBS) pH 7.4; and two phosphate buffers (PB) of different molarity and pH, 0.1 mol L^{-1} PB pH 8.0 and 0.05 mol L^{-1} PB pH 6.0. An EDC/Sulfo-NHS mixture solution (50 mg mL^{-1} each, prepared in MES buffer pH 5.0), a 1.0 M ethanolamine (ETA) solution (prepared in 0.1 mol L^{-1} PB pH 8.0) and 100 mM HQ and 100 mM H_2O_2 solutions (both in 0.05 mol L^{-1} PB pH 6.0) were prepared just before their use to ensure stability.

The standard and the antibody pair used for the determination of HE were those provided in the commercial ELISA kit: Human Endostatin DuoSet ELISA (Cat. No. DY1098 (15 plates), from R&D Systems) containing a recombinant HE standard, a mouse anti-HE capture antibody (cAb) and a biotinylated goat anti-HE detection antibody (b-dAb). Streptavidin-HRP (Strep-HRP) conjugate from Roche (Cat. No. 11089153001) was used as enzymatic tracer.

Albumin from human serum (HSA, Cat. No. A1653), IgG from human serum (hIgG, Cat. No. I2511), human haemoglobin (HB, Cat. No. H7379), all from Sigma-Aldrich, human Cadherin-17 (Cad-17, Cat. No. TP720740) from Origene, human TNFα (Cat. No. DY210) and human IL-13Rα2 from Human IL-13Rα2 DuoSet ELISA (Cat. No. DY614), from R&D Systems, were evaluated as possible interfering compounds.

2.3. Preparation of magnetic bioconjugates

The immunoassay on MBs involved successive incubation and washing steps of the MBs in 1.5 mL microcentrifuge tubes. These steps were performed in thermostatic incubators and under constant stirring (25 °C, 950 rpm). At the end of each step, the microcentrifuge tube with the MBs suspension was placed in the magnetic separator for 2 min before discarding the supernatant.

For each determination, a 1.5 mL microcentrifuge tube with a 3 μL aliquot of the HOOC-MBs commercial suspension was used. HOOC-MBs were washed twice for 10 min with 50 μL MES buffer. The carboxylic groups of the MBs surface were then activated by incubation for 35 min with 25 μL of a freshly prepared EDC/Sulfo-NHS solution. The activated HOOC-MBs were washed twice with MES buffer and incubated for 45 min in 25 μL of a 5 μg mL^{-1} cAb solution prepared in MES buffer. The cAb-MBs were washed twice with MES buffer and incubated in 1.0 M ETA solution for 60 min to block residual activated groups after cAb - immobilization. Finally, the modified MBs were washed with 0.1 M Tris − HCl buffer (pH 7.2) and twice with BB. The cAb-MBs could be used for determination at the time of preparation or stored (filtered PBS, 4 °C) for later use.

HE determination involved the formation of sandwich immunocomplexes following three successive steps of incubation of cAb-MBs with solutions of the standard target protein (in BB) for 45 min, 1 μg mL^{-1} of b-dAb (in BB), 15 min, and 1:1000 of Strep-HRP (in BB), 15 min.

MBs bearing the HRP-labelled sandwich immunocomplexes were washed twice with BB and resuspended in 50 μL of PB pH 6.0 for amperometric measurements.

2.4. Amperometric measurements

The SPCE (a new one for each measurement) was previously placed in the Nd magnet embedded-PMMA housing. 50 μL of the modified MBs suspension, prepared as detailed in the preceding section, were deposited on the working electrode surface. The housing/electrode assembly was immersed into a cell containing 10 mL of PB buffer pH 6.0 and 100 μL of freshly prepared 0.1 mol L^{-1} HQ solution. Amperometric detection was started, under continuous stirring, by applying a constant potential of −0.20 V *vs.* the Ag pseudo-reference electrode.

When the background current was stabilized, 50 μL of 0.1 mol L^{-1} H_2O_2 were added to the measuring cell and the current variation, attributed to the HQ-mediated enzymatic reduction of H_2O_2 was recorded until the signal was stabilized. The amperometric response was measured as the difference between the steady-state and the background currents obtained after and before the addition of H_2O_2, respectively. Values taken as electrochemical responses were the mean value of three replicates and the error bars were estimated as three times the standard deviation of these replicates ($\alpha = 0.05$).

2.5. Analysis of cellular and human samples

Plasma and tissue samples from healthy individuals and CRC patients were provided by the biobank of the Hospital Clínico San Carlos after approval of the Ethical Review Boards of this institution (CEI PI 45) and stored at −80 °C until use. Samples were used accomplishing all the ethical issues and relevant guidelines and regulations for sample handling and experiments performance. All individuals gave their written informed consent to participate in the study. Paired healthy and tumoral colon tissue biopsies from the same CRC patients at different stages of the disease were obtained in parallel during surgery.

Two isogenic CRC cell models with the same genetic background but different metastatic properties were used. The isogenic poorly metastatic KM12C cells, highly metastatic to liver KM12SM cells, and highly metastatic to liver and lung KM12L4a cells, were obtained from I. Fidler's laboratory (MD Anderson Cancer Center). Isogenic low-metastatic SW480 cells and highly metastatic to lymphatic nodes SW620 cells were from the American Type Culture Collection (ATCC) [17,18]. The protocols used to grow these cells are described in detail in a previous work [19]. Protein extracts from tissue samples and CRC cells were obtained as previously described, and the presence of HE was analysed by Western blot (WB) or Dot blot (DB) [19]. Briefly, cells and tissue samples (200 μg approximately) were lysed with 500 μL of RIPA buffer (Sigma) supplemented with 1× protease and phosphatase inhibitors (MedChemExpress) 1:100 diluted, and manually disaggregated until homogeneity was observed. Then, protein extracts were centrifuged at 10000*g* at 4 °C for 15 min, and supernatants (protein extracts) were transferred to a new tube and stored at −80 °C until use. Protein concentration in the extracts was calculated using the tryptophan method [20]. For WB analysis, 10 μg of each protein extract were separated in 10% SDS-PAGE under reducing conditions and transferred to a nitrocellulose membrane at 100 V for 90 min. For DB analysis, 40–60 μg of each cell secretome in 100 μL PBS were dot blotted onto nitrocellulose membranes using the Bio-Dot 96-Well Microfiltration (Bio-Rad). Then, nitrocellulose membranes were blocked with 3% skimmed milk 0.1% Tween PBS 1× (blocking buffer) for 1 h at room temperature (RT) and incubated overnight (O/N) at 4 °C, both steps in rotation, with the corresponding primary antibody 1:1000 diluted in blocking buffer (Anti-HE cAb; Anti-GAPDH, SCBT, sc-32233). Next, membranes were washed three times with 0.1% Tween PBS 1× (wash buffer) and incubated with an HRP anti-mouse polyclonal antibody (Sigma-Aldrich, A4416) 1 h at RT and in rotation. Signal was developed using the ECL Pico Plus chemiluminescent reagent (Thermo Fisher Scientific) and detected on an Amersham Imager 680 (GE Healthcare). GAPDH was used as loading control. Protein signal intensities were quantified using the ImageJ software and normalized according to their corresponding low-metastatic isogenic CRC cell line (KM12C or SW480 cells).

The possible existence of matrix effect in the analysis of these four biological matrices with the immunoplatform was evaluated. At the tested concentrations levels, matrix effect only occurred with the tissue samples, so that the determination in such samples was carried out by applying the standard additions method using 0.05 μg of tissue.

The determination of HE in plasma, secretomes, and cell extracts was carried out by simple interpolation of the amperometric responses obtained with 150- and 75- times diluted plasma and secretome samples, respectively, as well as with 0.1 μg of cell extracts.

3. Results and discussion

Scheme 1 displays the protocols for the preparation and transduction of the developed immunoplatform. They involve the formation of sandwich immunocomplexes labelled with the HRP enzyme on the surface of MBs, and the amperometric transduction on SPCEs using the H_2O_2/HQ system. The target protein (HE) was selectively captured by covalently immobilizing the capture antibody (cAb) on HOOC-MBs activated with EDC/Sulfo-NHS and blocked with ETA and detected with a biotinylated antibody (b-dAb) enzymatically labelled with a commercial Strep-HRP conjugate. According to the type of immunoassay, the resulting cathodic current variation was directly proportional to the concentration of HE.

3.1. Optimization of key experimental variables

The variables involved in the preparation of the immunoplatform were optimized by comparing the amperometric responses obtained in the presence of HE (500 pg mL^{-1}, S) and in its absence (B), and taking their ratio (S/B ratio) as the selection criterion. The results obtained for the variables tested are shown in Fig. 1 and summarized in Table 1. Other variables involved in the amperometric transduction (applied potential, concentrations of enzyme substrate and redox mediator, and composition and pH of the supporting electrolyte) were previously optimized [21].

First, the concentration and incubation time of the cAb solution for immobilization on activated MBs were evaluated (panels **a)** and **b)** in Fig. 1**a**). Larger S/B ratios were obtained by incubating the MBs in a 5 μg mL^{-1} cAb solution for 45 min. As can be observed, higher concentrations and longer incubation times resulted in lower S/B ratios due to a lower efficiency in the recognition of the target antigen when a large amount of cAb molecules were immobilized on the MBs [22].

A key variable is the number of protocol steps involved in the formation of the sandwich immunocomplexes. Three different protocols, using different 30 min incubation steps starting from cAb-MBs, were tested:

- Protocol I: A single incubation step in a mixed solution of HE, b-dAb and Strep-HRP.
- Protocols II(A) and II(B): Two successive incubation steps. While in II (A), the first incubation was in a mixed solution of HE and b-dAb, and the second incubation was with a Strep-HRP solution, in protocol II (B), the first incubation was with the HE solution and the second with a mixed solution of b-dAb and Strep-HRP.
- Protocol III: Three successive incubation steps with HE, b-dAb and Strep-HRP solutions.

According to the results shown in **panel c)** of Fig. 1, a larger S/B ratio was obtained using protocol III. This can be attributed to multiple factors including possible aggregation phenomena when working with mixtures of all bioreagents, lower recognition of the target by b-dAb when it is already conjugated with Strep-HRP and/or competition between cAb and b-dAb, particularly relevant if both bind to epitopes located close to each other in the protein, or in limiting concentrations of

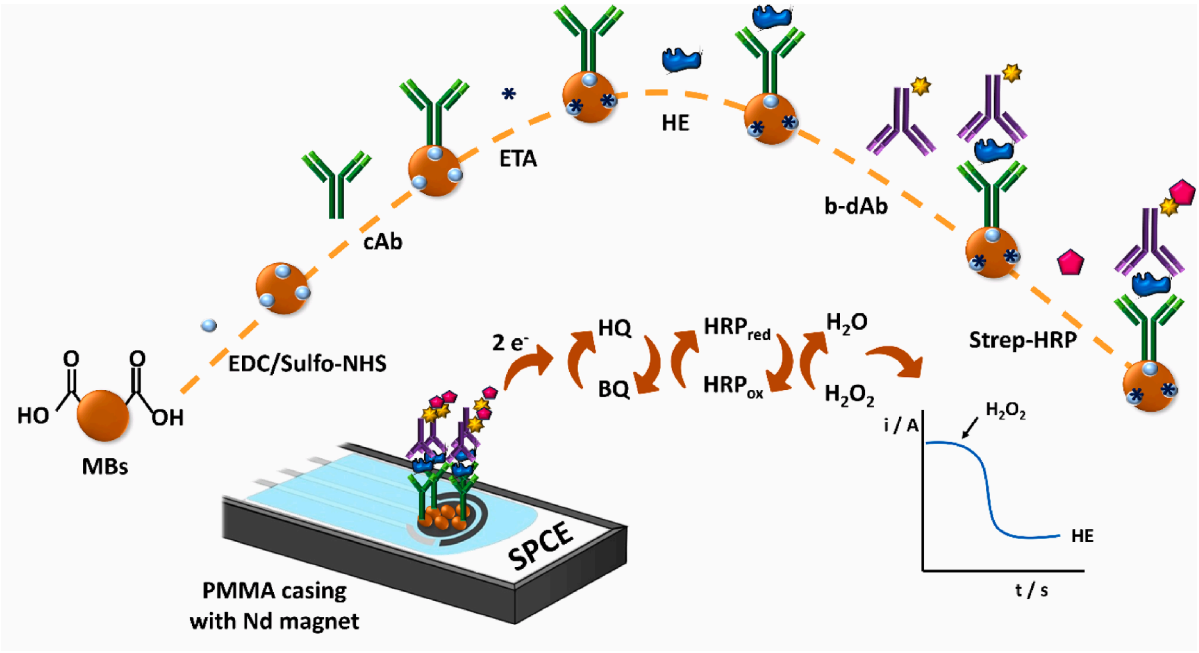

Scheme 1. Schematic diagram of the steps involved in the preparation of HE sandwich immunocomplexes on the surface of MBs and the amperometric transduction after their magnetic capture on the SPCE working electrode.

analyte or one of the antibodies.

The optimization of the other experimental variables led to the selection of incubation times of 45 min for the HE solution (Fig. 1**d**), and concentrations/dilutions and incubation times of 1 μg mL^{-1} and 30 min for the b-dAb solution (Fig. 1**e and f**) and 1/1000 and 15 min for Strep-HRP (Fig. 1**g** and **h**), respectively.

These optimization results further confirmed that discrimination of the presence of the target protein was not possible in the absence of cAb or b-dAb (bars 0 in panels **a)** and **e)** of Fig. 1), and therefore that the determination of HE took place through the formation of sandwich immune complexes.

3.2. Immunoplatform operational characteristics

The analytical characteristics of the developed HE immunoplatform are summarized in Table 2. Under the optimized working conditions shown in Table 1, a calibration plot was constructed for HE standards in buffered solutions (Fig. 2)**.** A linear dependence between the amperometric signals and the target protein concentration ($R^2 = 0.9921$) was obtained over the 114–1000 pg mL^{-1} HE concentration range, fitting the equation - i, nA = (0.09 ± 0.02) nA mL pg^{-1} [HE] + (73 ± 2) nA.

The limit of detection (LOD) and quantification (LOQ) values were estimated according to the 3 × s_b/slope and 10 × s_b/slope criteria (where s_b was the standard deviation of ten B amperometric measurements). The calculated values were 34.1 and 113.6 pg mL^{-1}, respectively.

The bioplatform achieved LOD values around three-four orders of magnitude lower than the HE levels in plasma reported in the literature for healthy individuals and CRC patients (mean values of 43.2 and 71.6 ng mL^{-1}, respectively [6]).

The reproducibility of the measurements carried out with the developed immunoplatform was checked by comparing the responses obtained with ten different bioplatforms prepared on the same day for 500 pg mL^{-1} HE. A relative standard deviation (RSD) value of 3.94 % was obtained, thus confirming the reproducibility of the protocols used both for the preparation of the immunocomplexes and for the amperometric transduction after their capture on the SPCE working electrode. Regarding storage stability, the cAb-MBs, were resuspended, after the blocking step, in 10 mM filtered PBS and stored at 4 °C. Thereafter, they were used to measure every testing day the amperometric responses provided by the immunoconjugates using the stored cAb-MBs after incubation in 0.0 and 500 pg mL^{-1} HE solutions. Such amperometric responses remained within the control limits for 13 days, without a significant loss of sensitivity, suggesting that the cAb-MBs can be stored for almost two weeks until the determination needs to be made.

3.3. Selectivity

The selectivity of the immunoplatform was evaluated by comparing the amperometric signals measured for 0 (white bars) and 500 pg mL^{-1} (blue bars) HE standards in the absence and in the presence of potential interfering proteins (hIgG, HSA, Hb, Cad-17, IL-13Rα2 and TNF) which can be found in human serum. The assayed concentration levels are those expected in healthy individuals (see Fig. 3 caption). Moreover, the supplier company of the employed DY1098 DuoSet ELISA (HE immunoreagents) certified no cross-reactivity for recombinant human Angiopoietin-2, Ephrin-A5/Fc Chimera and Tie-2/Fc Chimera, all tested at the 50 ng mL^{-1} concentration level.

As can be seen in Fig. 3, only hIgG and HSA interfered with HE determination at the highest concentrations tested. The interference observed with hIgG should be attributed to nonspecific adsorptions of hIgGs on the surface of MBs [23]. Moreover, some studies have shown that HSA, unless highly purified, may contain hIgGs that can disturb the assay for the same reason. This type of interference for HSA concentrations equal to or greater than 5 mg mL^{-1} has been described in other sandwich immunoassays [24,25]. However, as expected, these two interferences can be minimized after appropriate dilution, 10-fold for hIgG or 100-fold for HSA. It is also important to point out that the presence of these potential interferences as well as their concentration depend on the type of clinical sample analyzed.

3.4. Analysis of clinical samples

To deepen the role of HE and angiogenesis in CRC, the developed bioplatform was applied to the analysis of five CRC cells extracts and secretomes with different metastatic capacities, as well as to sixteen

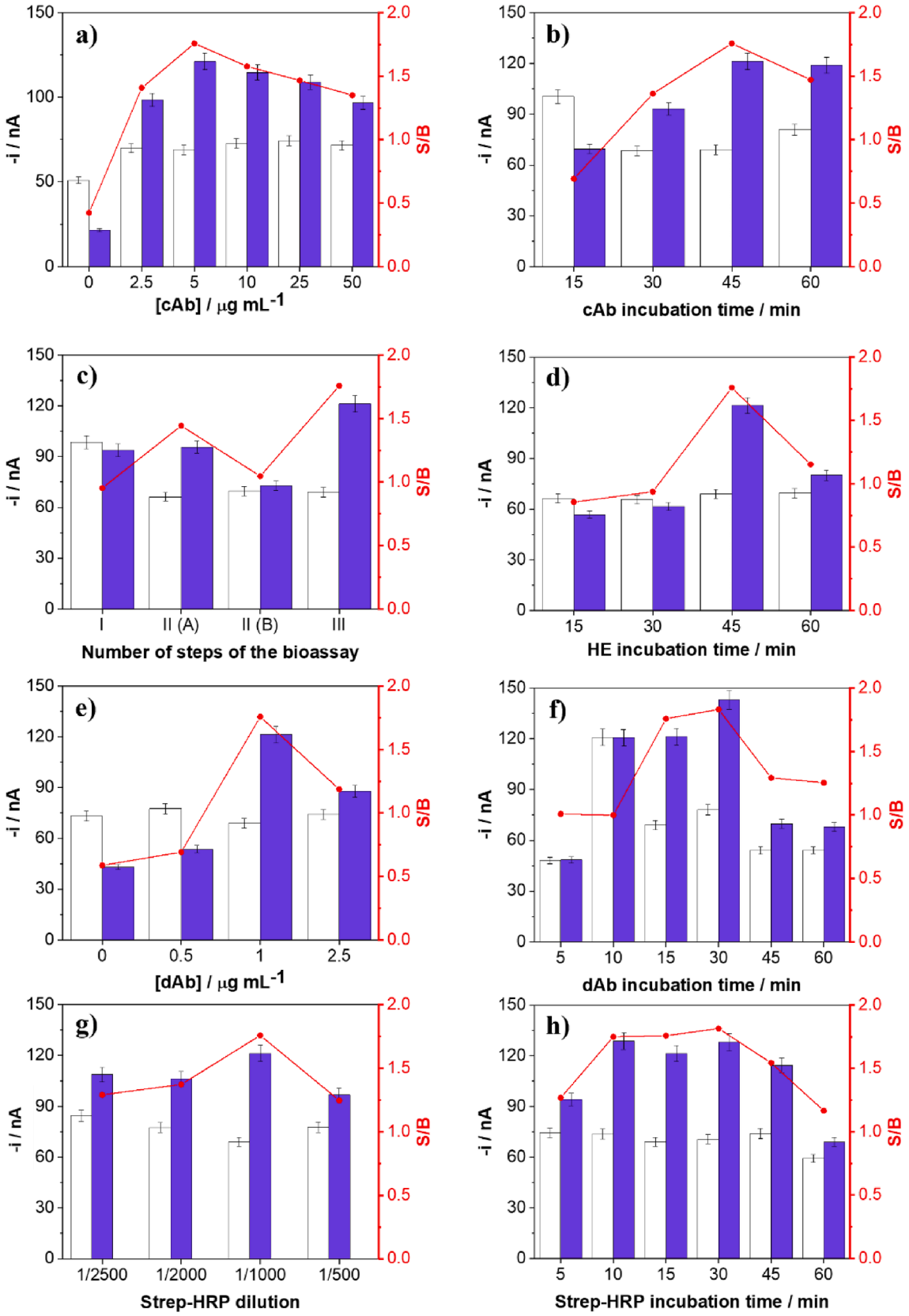

Fig. 1. Dependence of the amperometric responses measured with the developed immunoplatform in the absence (white bars, B) and in the presence (blue bars, S) of 500 pg mL^{-1} HE, and the resulting S/B ratios (red dots and line) with the concentration (a) and incubation time (b) of the cAb solution, the number of steps involved in the preparation of the bioconjugates (c), the incubation time with HE (d), the concentration (e) and incubation time (f) with the b-dAb solution, and the dilution (g) and incubation time (h) with the Strep-HRP solution.

Table 1
Optimization of the key experimental variables involved in the determination of HE with the developed amperometric immunoplatform.

Variable	Tested Range	Selected value
[cAb], μg mL^{-1}	0.0–50.0	5.0
cAb incubation time, min	15–60	45
Number of steps of the bioassay	1–3	3
HE incubation time, min	15–60	45
[b-dAb], μg mL^{-1}	0.0–2.5	1.0
b-dAb incubation time, min	5–60	15
Strep-HRP dilution	1/2500–1/500	1/1000
Strep-HRP incubation time, min	5–60	15

Table 2
Analytical characteristics offered by the developed immunoplatform for the amperometric determination of HE.

Parameter	Value
Linear range, pg mL^{-1}	114–1000
Slope, nA mL pg^{-1}	0.09 ± 0.02
Intercept, nA	73 ± 2
R^2	0.9921
LOD, pg mL^{-1}	34.1
LOQ, pg mL^{-1}	113.6
$RSD_{n=10}$, %	3.9

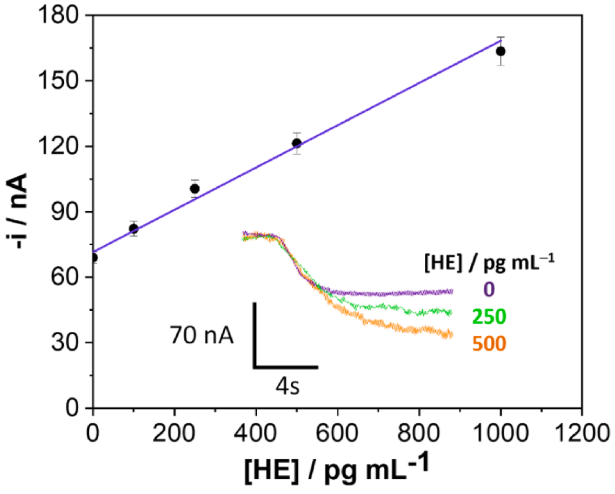

Fig. 2. Calibration graph constructed for the determination of HE with the developed bioplatform. Inset: real amperometric traces recorded.

liquid (plasma) and needle (tissue) biopsies of patients diagnosed with CRC in different stages. While the determination of biomarkers in cell lysates and secretomes, particularly in the latter, is currently considered an ideal alternative for biomarker identification and elucidation of their role in carcinogenesis without sacrificing valuable clinical samples [26], their simultaneous interrogation in liquid and needle biopsy samples is considered of great relevance both to improve the reliability of the determination and to provide a much more complete picture of both solid and circulating disease.

Firstly, the suitable amount of sample and the possible existence of a matrix effect in the different biological samples to be analyzed were evaluated. Therefore, the slope values of the calibration plots constructed with HE standards in buffered solutions and in the different clinical samples were statistically compared [27]. The results summarized in Table S1 (in the Supplementary Information), show that working with the indicated concentrations/dilutions (0.05 μg of tissues, 0.1 μg of cell extracts, and samples of plasma and secretomes diluted 150 and 75 times, respectively), only a matrix effect ($t_{exp} > t_{tab}$) was found for the tissues determination.

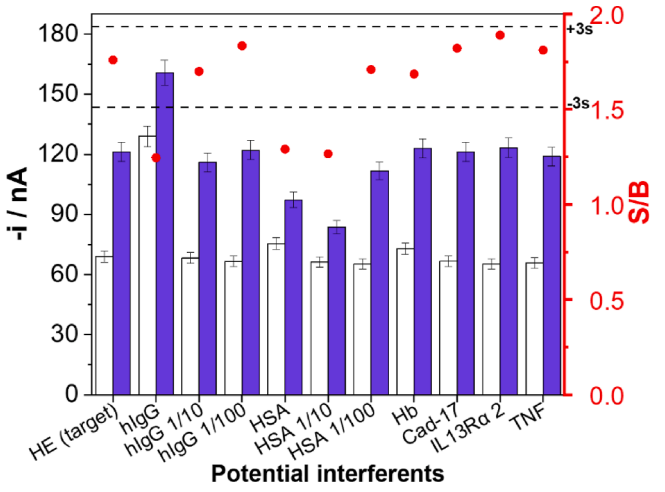

Fig. 3. Amperometric responses provided by the immunoplatform for 0 (white bars) and 500 pg mL^{-1} HE (blue bars) standards prepared in the absence and in the presence of 1 mg mL^{-1} hIgG, 0.1 mg mL^{-1} hIgG, 0.01 mg mL^{-1} hIgG, 50 mg mL^{-1} HSA, 5 mg mL^{-1} HSA, 0.5 mg mL^{-1} HSA, 5 mg mL^{-1} Hb, 500 ng mL^{-1} Cad-17, 10 ng mL^{-1} IL-13Rα2 and 100 pg mL^{-1} TNF. S/B ratio values displayed in red dots and control limits (dashed black lines) were set as ± 3 s of the mean value of three bioplatforms.

Accordingly, as detailed in Section 2.4, the determination of HE in tissues were carried out by applying the standard additions method, while a simple interpolation of the amperometric responses into the calibration graph constructed with standards in buffered solutions (Fig. 2) was used for plasma, cells extracts and secretomes. The results obtained in these determinations are shown in Figs. 4 and 5 and summarized in Tables 3 and 4.

The results obtained with the bioplatform for the extracts and secretomes of CRC cells (panels a and b in Fig. 4) show the presence of larger HE concentrations in the cells with higher metastatic potential (SW620, KM12L4a and KM12SM). It is also noteworthy that the expression relationships between the SW620/SW480 and KM12SM/KM12C isogenic pairs (pair of cells differing only in a single genetic alteration) were consistent in both types of samples and larger in the second isogenic pair. These results were also consistent with the semi-quantitative results obtained by dot-blot (panels **c)** and **d)** in Fig. 4) as well as with those reported by Chung *et al.* [28] in extracts of the SW620/SW480 pair by Western analysis (3.59/1.11).

Regarding the determinations in plasma and tissues of CRC patients in different stages, the results shown in Fig. 5**a)** and in Table 4, indicated significantly higher plasma levels of HE in CRC patients compared to healthy individuals. Moreover, the HE level in both plasma and tissues appeared to be related to the course of the disease. These results agreed with the fact that, despite its recognized antiangiogenic functions, elevated concentrations of circulating HE have been found in several human cancers and have been associated with advanced stages and poorer prognosis [7], and in the case of plasma with the established cut-off value (73.4 ng mL^{-1}) in CRC patients [6].

In the case of tissue samples (Fig. 5**b**), it is remarkable the consistency between the concentrations found in the healthy tissue samples of the 8 CRC patients analyzed and between the contents found in the tumor tissue samples at the same stages of the disease. Moreover, as in the plasma samples, the expression of HE increases with the progression of the disease, moving the T/NT ratio (in Table 4) within the range 1.2–1.7.

Importantly, the ROC curve analysis of the results obtained with the four types of analyzed samples (**Fig. S1** in the Supplementary Information), confirms that it is possible to clearly discriminate the metastatic capabilities of cancer cells through the determination of HE in their extracts or exosomes and between healthy subjects and CRC patients by

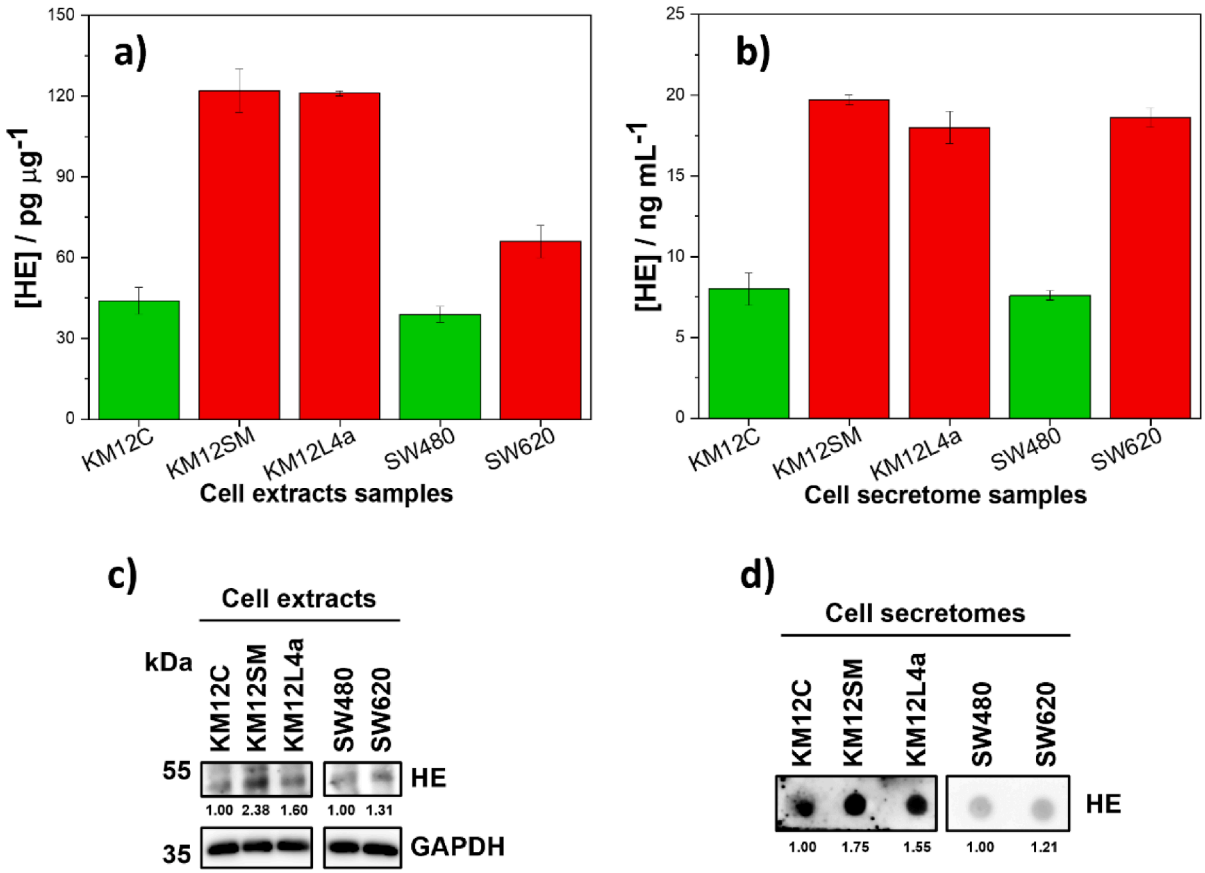

Fig. 4. Results obtained with the developed bioplatform (a, b) and WB (c) and DB (d) analysis for the determination of HE in cell extracts (a, c) and secretomes (b, d) from CRC cells with different metastatic abilities. ImageJ was used for the semi-quantitation of HE shown in (c) and (d). Protein bands were normalized using GAPDH (c).

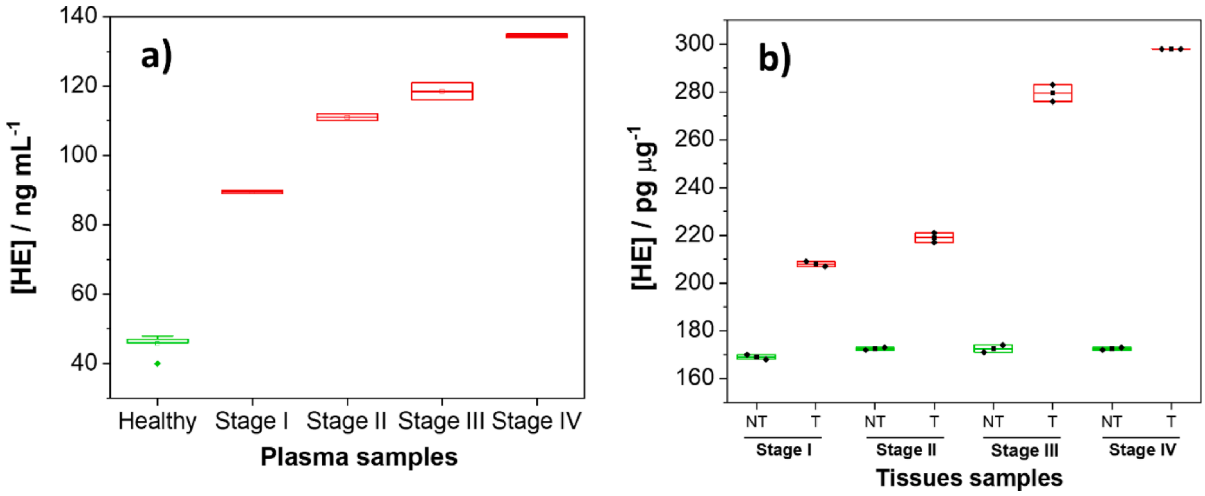

Fig. 5. Results obtained with the bioplatform for the determination of HE in plasma from healthy subjects (green) and from CRC patients in different stages (red) (a), and from paired healthy (green) and tumor (red) tissues of CRC patients in different stages (b).

analyzing tissue or plasma samples.

It is important to note that the ROC curves analysis of the results obtained for tissue and plasma samples of healthy individuals and CRC patients at different stages confirm the potential of the bioplatform to assist in CRC staging through the determination of HE (see the parameters summarized in **Table S2** in the Supplementary Information).

Moreover, in addition to provide the first quantitative results for the determination of HE in CRC cell secretomes and CRC patients samples, the obtained results confirm the potential of the proposed electrochemical bioplatform for the determination of the same target both in cells and in liquid biopsies and tissues. This is particularly relevant in the case of HE (with known antitumor and antiangiogenic effects for its recombinant form) [29–31] but whose natural circulating levels are also associated with advanced stages and worse prognosis in certain types of cancer [7]). Indeed, there is evidence that elevated HE levels in CRC may be released by invasive cancer cells cleaving endostatin from collagen

Table 3
Determination of endostatin in extracts and secretomes of CRC cells with different metastatic capacities.

Cell	Metastatic ability	Extracts (0.1 μg)			Secretomes (1/75)		
		[HE], $pg\mu g^{-1}$*	M/NM	$RSD_{n=3}$, %	[HE], ng mL^{-1}*	M/NM	$RSD_{n=3}$, %
SW480	NM	39 ± 3	1.7	2.9	7.6 ± 0.3	1.7	1.3
SW620	M	66 ± 6		3.6	18.6 ± 0.6		1.4
KM12C	NM	44 ± 5	2.8	4.4	8 ± 1	2.5	6.9
KM12SM	M	122 ± 8		2.7	19.7 ± 0.3		0.7
KM12L4a	M	121 ± 1	–	0.3	18 ± 1	–	3.0

*mean value ± $ts/\sqrt{n}$; n = 3; α = 0.05. M: metastatic; NM: non-metastatic.

Table 4
Results obtained in the determination of endostatin with the bioplatform in plasma samples from healthy individuals and CRC patients in different stages, and in paired tissues (non-tumoral, NT, and tumoral, T) from patients diagnosed with CRC in different stages.

Plasma samples				Tissue samples				
Sample	Subject	[HE], ng mL^{-1}*	$RSD_{n=3}$, %	Sample (CRC Stage)	Tissues type	[HE], $pg\mu g^{-1}$*	T/NT	$RSD_{n=3}$, %
1	Healthy	40 ± 3	3.1	1 (I)	NT	170 ± 6	1.2	1.3
2		47 ± 2	1.7		T	209 ± 10		2.0
3		46 ± 4	3.4	2 (I)	NT	168 ± 10	1.2	2.4
4		47 ± 4	3.8		T	207 ± 3		0.6
5		46 ± 1	1.2	3 (II)	NT	173 ± 13	1.3	3.1
6		46 ± 3	2.9		T	217 ± 8		1.5
7		46 ± 1	1.2	4 (II)	NT	172 ± 15	1.3	3.5
8		48 ± 3	2.6		T	221 ± 18		3.4
9	CRC (I)	90 ± 8	3.4	5 (III)	NT	171 ± 10	1.6	2.2
10		89 ± 2	1.0		T	283 ± 6		0.8
11	CRC (II)	110 ± 7	2.6	6 (III)	NT	174 ± 9	1.6	2.1
12		112 ± 2	0.6		T	276 ± 7		1.0
13	CRC (III)	116 ± 4	1.4	7 (IV)	NT	173 ± 6	1.7	1.5
14		121 ± 3	1.1		T	298 ± 4		0.6
15	CRC (IV)	135 ± 12	3.7	8 (IV)	NT	172 ± 13	1.7	3.1
16		134 ± 11	3.3		T	298 ± 13		1.8

* mean value ± $ts/\sqrt{n}$; n = 3; α = 0.05.

XVIII in the intestinal wall and correlate with systemic inflammation and invasion through the muscularis propria, but not with intratumoral mast cells and immature dendritic cells, possibly due to inhibition of angiogenesis by HE [7].

4. Conclusions

This work proposes the first bioplatform for the determination of HE based on the implementation of sandwich immunocomplexes, enzymatically labeled with HRP, on the surface of MBs and using amperometric transduction on SPCEs. This novel biotool provides suitable sensitivity (LOD of 34.1 pg mL^{-1}) and selectivity for clinical application. Indeed, the electrochemical bioplatform has been confronted with the analysis of lysates and secretomes of CRC cells and of plasma and tissue samples from CRC patients at different stages. The obtained results confirm the relationship of the HE expression with the cells aggressiveness and with the CRC stage. In addition, the developed bioplatform allows accurate determinations, that require minimal pretreatment and sample quantities, to be performed in only 75 min, and in four different matrices of high clinical relevance and complexity. This bioplatform, unlike the ELISA or immunoblotting technologies, is compatible with future implementation in multiplexed and/or point-of-need determination devices. Moreover, the developed methodology is readily transferable to the determination of other relevant markers to evaluate their diagnostic, prognostic and/or follow-up potential in oncological medicine. It is important to note that commercially available ELISA kits are recommended for HE determination in cell culture supernatant, serum and plasma, but not in cell and tissue extracts, samples of high complexity and great clinical relevance to which the developed bioplatform has been successfully applied.

Funding

The financial support of PID2019-103899RB-I00 (Spanish Ministerio de Ciencia e Innovación) Research Project and PI20CIII/00019 Grant from the AES-ISCIII Program co-founded by FEDER funds and the TRANSNANOAVANSENS-CM Program from the Comunidad de Madrid (Grant S2018/NMT-4349) are gratefully acknowledged. M.G-A. acknowledges the postdoctoral contract Margarita Salas for the requalification of the Spanish University System. A.M-C. was supported by a FPU predoctoral contract supported by the Spanish Ministerio de Educación, Cultura y Deporte. S.T.M. acknowledges a predoctoral contract from the Spanish Ministerio de Ciencia e Innovación (PRE2020-092859).

Declaration of Competing Interest

The authors declare that they have no known competing financial interests or personal relationships that could have appeared to influence the work reported in this paper.

Data availability

Data will be made available on request.

Appendix A. Supplementary data

Supplementary data to this article can be found online at https://doi.org/10.1016/j.bioelechem.2023.108571.

References

[1] G. Méndez-Valdés, F. Gómez-Hevia, J. Lillo-Moya, T. González-Fernández, J. Abelli, A. Cereceda-Cornejo, M.C. Bragato, L. Saso, R. Rodrigo, Endostatin and cancer therapy: a novel potential alternative to anti-VEGF monoclonal antibodies, Biomedicines 11 (2023) 718, https://doi.org/10.3390/biomedicines11030718.
[2] M.S. O'Reilly, T. Boehm, Y. Shing, N. Fukai, G. Vasios, W.S. Lane, E. Flynn, J. R. Birkhead, B.R. Olsen, J. Folkman, Endostatin: an endogenous inhibitor of

angiogenesis and tumor growth, Cell 88 (1997) 277–285, https://doi.org/10.1016/S0092-8674(00)81848-6.
[3] U.K. Zatterstrom, U. Felbor, N. Fukai, B.R. Olsen, Collagen XVIII/endostatin structure and functional role in angiogenesis, Cell Struct. Funct. 25 (2000) 97–101, https://doi.org/10.1247/csf.25.97.
[4] M.A. Grant, R. Kalluri, Structural basis for the functions of endogenous angiogenesis inhibitors, Cold Spring Harb. Symp. Quant. Biol. 70 (2005) 399–417, https://doi.org/10.1101/sqb.2005.70.017.
[5] M. Li, Z. Popovic, C. Chu, B.K. Krämer, B. Hocher, Endostatin in renal and cardiovascular diseases, Kidney Dis. 7 (2021) 468–481, https://doi.org/10.1159/000518221.
[6] A.L. Feldman, H.R. Alexander, D.L. Bartlett, K.C. Kranda, M.S. Miller, N. G. Costouros, P.L. Choyke, S.K. Libutti, A prospective analysis of plasma endostatin levels in colorectal cancer patients with liver metastases, Ann. Surg. Oncol. 8 (2001) 741–745, https://doi.org/10.1007/s10434-001-0741-x.
[7] T. Kantola, J.P. Väyrynen, K. Klintrup, J. Mäkelä, S.M. Karppinen, T. Pihlajaniemi, H. Autio-Harmainen, T.J. Karttunen, A. Tuomisto, Serum endostatin levels are elevated in colorectal cancer and correlate with invasion and systemic inflammatory markers, Br. J. Cancer 111 (2014) 1605–1613, https://doi.org/10.1038/bjc.2014.456.
[8] P. Nyberg, L. Xie, R. Kalluri, Endogenous inhibitors of angiogenesis, Cancer Res. 65 (2005) 3967–3979, https://doi.org/10.1158/0008-5472.CAN-04-2427.
[9] Y. Sato, Endostatin as a biomarker of basement membrane degradation, J. Atheroscler. Thromb. 24 (10) (2017) 1014–1015, https://doi.org/10.5551/jat.ED077.
[10] L. Ständker, M. Schrader, S.M. Kanse, M. Jürgens, W.-G. Forssmann, K.T. Preissner, Isolation and characterization of the circulating form of human endostatin, FEBS Lett. 420 (1997) 129–133, https://doi.org/10.1016/S0014-5793(97)01503-2.
[11] H. John, W.-G. Forssmann, Determination of the disulfide bond pattern of the endogenous and recombinant angiogenesis inhibitor endostatin by mass spectrometry, Rapid Commun. Mass Spectrom. 15 (2001) 1222–1228, https://doi.org/10.1002/rcm.367.
[12] L. Roussille, G. Brotons, L. Ballut, G. Louarn, D. Ausserré, S. Ricard-Blum, Surface characterization and efficiency of a matrix-free and flat carboxylated gold sensor chip for surface plasmon resonance (SPR), Anal. Bioanal. Chem. 401 (2011) 1601–1617, https://doi.org/10.1007/s00216-011-5220-z.
[13] M. Määttä, R. Heljasvaara, T. Pihlajaniemi, M. Uusitalo, Collagen XVIII/endostatin shows a ubiquitous distribution in human ocular tissues and endostatin-containing fragments accumulate in ocular fluid samples, Graefe's Arch. Clin. Exp. Ophthalmol. 245 (2007) 74–81, https://doi.org/10.1007/s00417-006-0281-y.
[14] Y.Y. Joo, J.W. Jang, S.W. Lee, S.H. Yoo, J.H. Kwon, S.W. Nam, S.H. Bae, J.Y. Choi, S.K. Yoon, Circulating pro- and anti-angiogenic factors in multi-stage liver disease and hepatocellular carcinoma progression, Sci. Rep. 9 (2019) 9137, https://doi.org/10.1038/s41598-019-45537-w.
[15] J. Mason, E. Lundberg, P. Jonsson, H. Nyström, O. Franklin, C. Lundin, P. Naredi, H. Antti, M. Sund, D. Öhlund, A cross-sectional and longitudinal analysis of pre-diagnostic blood plasma biomarkers for early detection of pancreatic cancer, Int. J. Mol. Sci. 23 (2022) 12969, https://doi.org/10.3390/ijms232112969.
[16] S. Campuzano, M. Gamella, M. Pedrero, J.M. Pingarrón, Affinity bioelectroanalysis in cellular-level biomarker driven modern precision cancer diagnosis, TrAC, Trends Anal. Chem. 163 (2023), 117064, https://doi.org/10.1016/j.trac.2023.117064.
[17] K. Morikawa, S.M. Walker, J.M. Jessup, I.J. Fidler, In vivo selection of highly metastatic cells from surgical specimens of different primary human colon carcinomas implanted into nude mice, Cancer Res. 48 (1988) 1943–1948.
[18] K. Morikawa, S.M. Walker, M. Nakajima, S. Pathak, J.M. Jessup, I.J. Fidle, Influence of organ environment on the growth, selection, and metastasis of human colon carcinoma cells in nude mice, Cancer Res. 48 (1988) 6863–6871.
[19] C. Muñoz-San Martín, A. Montero-Calle, M. Garranzo-Asensio, M. Gamella, V. Perez-Gines, M. Pedrero, J.M. Pingarrón, R. Barderas, N. de-los-Santos-Alvarez, M.J. Lobo-Castañón, S. Campuzano, First bioelectronic immunoplatform for quantitative secretomic analysis of total and metastasis-driven glycosylated haptoglobin, Anal. Bioanal. Chem. 415 (2023) 2045–2057, https://doi.org/10.1007/s00216-022-04397-6.
[20] J.R. Wisniewski, F.Z. Gaugaz, Fast and sensitive total protein and peptide assays for proteomic analysis, Anal. Chem. 87 (2015) 4110–4116, https://doi.org/10.1021/ac504689z.
[21] M. Eguilaz, M. Moreno-Guzmán, S. Campuzano, A. González-Cortés, P. Yañez-Sedeño, J.M. Pingarrón, An electrochemical immunosensor for testosterone using functionalized magnetic beads and screen-printed carbon electrodes, Biosens. Bioelectron. 26 (2) (2010) 517–522, https://doi.org/10.1016/j.bios.2010.07.060.
[22] U. Eletxigerra, J. Martinez-Perdiguero, S. Merino, R. Villalonga, J.M. Pingarrón, S. Campuzano, Amperometric magnetoimmunoassay for the direct detection of tumor necrosis factor alpha biomarker in human serum, Anal. Chim. Acta 838 (2014) 37–44, https://doi.org/10.1016/j.aca.2014.05.047.
[23] B. Arévalo, V. Serafín, M. Garranzo-Asensio, R. Barderas, P. Yáñez-Sedeño, S. Campuzano, J.M. Pingarrón, Early and differential Çautoimmune diseases diagnosis by interrogating specific autoantibody signatures with multiplexed electrochemical bioplatforms, Biosen. Bioelectron.: X 13 (2023) 100325, 10.1016/j.biosx.2023.100325.
[24] R.-N. Zhao, Z. Feng, Y.-N. Zhao, L.-P. Jia, R.-N. Ma, W. Zhang, L. Shang, Q.-W. Xue, H.-S. Wang, A sensitive electrochemical aptasensor for Mucin 1 detection based on catalytic hairpin assembly coupled with PtPdNPs peroxidase-like activity, Talanta 200 (2019) 503–510, https://doi.org/10.1016/j.talanta.2019.03.012.
[25] V. Pérez-Ginés, R. M. Torrente-Rodríguez, A. Montero-Calle, G. Solís-Fernández, P. Atance-Gómez, M. Pedrero, J. M. Pingarrón, R. Barderas, S. Campuzano, Tackling CD147 exosome-based cell-cell signaling by electrochemical biosensing for early colorectal cancer detection, Biosens. Bioelectron.: X, 11 (2022) 100192, 10.1016/j.biosx.2022.100192.
[26] C.-C. Wu, C.-W. Hsu, C.-D. Chen, C.-J. Yu, K.-P. Chang, D.-I. Tai, H.-P. Liu, W.-H. Su, Y.-S. Chang, J.-S. Yu, Candidate serological biomarkers for cancer identified from the secretomes of 23 cancer cell lines and the Human Protein Atlas, Mol. Cell. Proteomics 9 (6) (2010) 1100–1117, https://doi.org/10.1074/mcp.M900398-MCP200.
[27] J.M. Andrade, M.G. Estévez-Pérez, Statistical comparison of the slopes of two regression lines: a tutorial, Anal. Chim. Acta 838 (2014) 1–12, https://doi.org/10.1016/j.aca.2014.04.057.
[28] S. Chung, S. Dwabe, Y. Elshimali, H. Sukhija, C. Aroh, J.V. Vadgama, Identification of novel biomarkers for metastatic colorectal cancer using angiogenesis-antibody array and intracellular signaling array, PLoS One 10 (8) (2015) e0134948.
[29] A. Walia, J.F. Yang, Y.-H. Huang, M.I. Rosenblatt, J.-H. Chang, D.T. Azar, Endostatin's emerging roles in angiogenesis, lymphangiogenesis, disease, and clinical applications, Biochim. Biophys. Acta 2015 (1850) 2422–2438, https://doi.org/10.1016/j.bbagen.2015.09.007.
[30] K. Zhang, Y. Wang, X. Yu, Y. Shi, Y. Yao, X. Wei, X. Ma, Recombinant human endostatin combined with radiotherapy inhibits colorectal cancer growth, BMC Cancer 17 (2017) 899, https://doi.org/10.1186/s12885-017-3903-3.
[31] K. Li, M. Shi, S. Qin, Current status and study progress of recombinant human endostatin in cancer treatment, Oncol. Ther. 6 (2018) 21–43, https://doi.org/10.1007/s40487-017-0055-1.